Nanoparticle Targeting

DOI: 10.1002/anie.201003445

Ligand-Clustered "Patchy" Nanoparticles for Modulated Cellular Uptake and In Vivo Tumor Targeting**

*Zhiyong Poon, Shujun Chen, Amanda C. Engler, Hyung-il Lee, Evrim Atas, Geoffrey von Maltzahn, Sangeeta N. Bhatia, and Paula T. Hammond**

Many biological systems interact through multiple simultaneous interactions.[1–3] While it is well acknowledged that, on the macroscale, these multivalent interactions strongly influence ligand–receptor binding kinetics and the biological responses they govern, the microscale patterning of ligands on substrates can also have a profound effect on multivalent kinetics and are able to further modulate biological signaling.[4] In particular, ligand–receptor clusters can substantially increase interactions between cell and substrate; not only the valency, but spatial factors such as branching mode and the localized clustering of groups are important[5–7] in influencing binding and downstream signaling processes.[8,9] Still, despite the prevalence of patterned ligand presentation found in cell biology and its demonstrated significance on 2D tissue engineering formats,[10,11] it remains largely unappreciated in the design of nanoparticle synthetic systems intended to interact with cells.

Traditionally, ligands have been attached in moderate to large quantities to liposomes, inorganic nanoparticles, and linear–linear block copolymer micelles;[12,13] however, typically they are presented in a randomly distributed fashion across the nanoparticle surface from a linear tether, typically polyethylene glycol (PEG), in a structure that does not enable manipulation of ligands in specific groupings with control of cluster group size and spacing. We hypothesized that precise control over the elements promoting and controlling multivalent presentation on targeted therapeutic carriers could enhance the efficacy and specificity of targeted delivery. To test this hypothesis, scaffolds that are able to localize a variable number of ligands within confined regions are required; this requirement cannot be satisfied by traditional material systems used in targeted delivery[14] such as linear–linear block polymers and PEG-functional liposomes. Here, we introduce the use of a systematic and informed linear dendritic design for a new modular polymer delivery system that can generate clustered or patchy presentations of ligand on micellar surfaces.[15] We demonstrate the use of prefunctionalized linear dendritic polymers (LDPs) in forming mixed micelle formulations that present different spatial arrangements of variable sized ligand clusters and examine the targeting efficacy of these formulations in vitro and in vivo. This new approach to ligand presentation on a nanoparticle surface enables the targeting community to probe means of enhancing cell selectivity at low to moderate ligand concentrations with greatly enhanced uptake. It also provides a tool for the exploration of cellular interactions with nanoscale-patterned ligands.

The design of the LDP is based on drug delivery principles, and each component is either fully biodegradable or biocompatible (Figure 1a). Hydrophobic PBLA (polybenzyl-L-aspartate) forms the polypeptide linear block to which a generation four hydrolytically degradable polyester dendron is attached. The sixteen end branches of the dendron are extended with sixteen short hydrophilic PEG chains. The degree of polymerization of PBLA is approximately 12 and the PEG branches have molecular weights of approximately 600 g mol^{-1}. The well-characterized model ligand folate,[16]

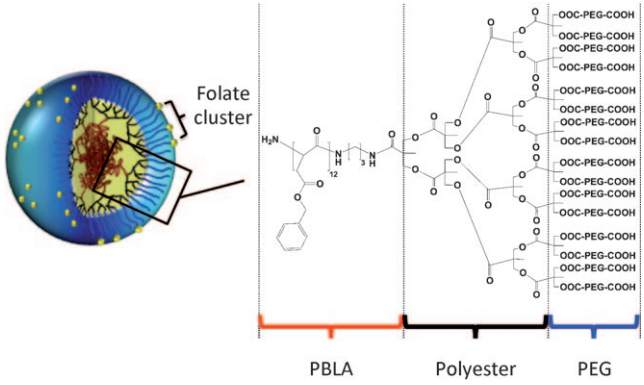

Figure 1. Chemical structure and self-assembly of linear dendritic polymers (LDP). Detailed chemical structure of the non-folate conjugated linear dendritic polymer and illustration of its self-assembly into "patchy" micelles presenting clusters of folate of variable sizes on the surface of the micelle. PBLA = poly(benzyl-L-aspartic acid), PED = polyester dendron, PEG = poly(ethylene glycol).

[*] Z. Poon, S. Chen, A. C. Engler, H. Lee, E. Atas, Prof. P. T. Hammond
Department of Chemical Engineering
Massachusetts Institute of Technology
77 Massachusetts Avenue, Cambridge, MA 02139 (USA)
Fax: (+1) 617-258-7577
E-mail: hammond@mit.edu
H. Lee
Department of Chemistry, University of Ulsan
Ulsan 680-749 (Republic of Korea)
G. von Maltzahn, Prof. S. N. Bhatia
Harvard-MIT Division of Health Science and Technology
Massachusetts Institute of Technology (USA)

[**] This work was funded by the National Institute of Health (NIH NIBIB grant 5R01EB008082-02), the MIT Center for Cancer Nanotechnology Excellence, and the National Science Foundation. We also wish to thank the Koch Institute for Integrative Cancer Research, Institute of Soldier Nanotechnologies (ISN), and the Center for Material Science and Engineering (CMSE) for use of facilities and equipment.

Supporting information (including experimental details) for this article is available on the WWW under http://dx.doi.org/10.1002/anie.201003445.

which is conjugated to the free PEG end through dicyclohexylcarbodiimide/*N*-hydroxysuccinimide (DCC/NHS) chemistries, was selected for this study. Using the model ligand folate, a range of ligand functionalization on the dendron was confirmed by both ^{1}H NMR and UV/Vis spectroscopy, which allows the expression of different folate cluster size ranges on the micelle surface (Figure 2a and Figures S1, S2a, S2c in the

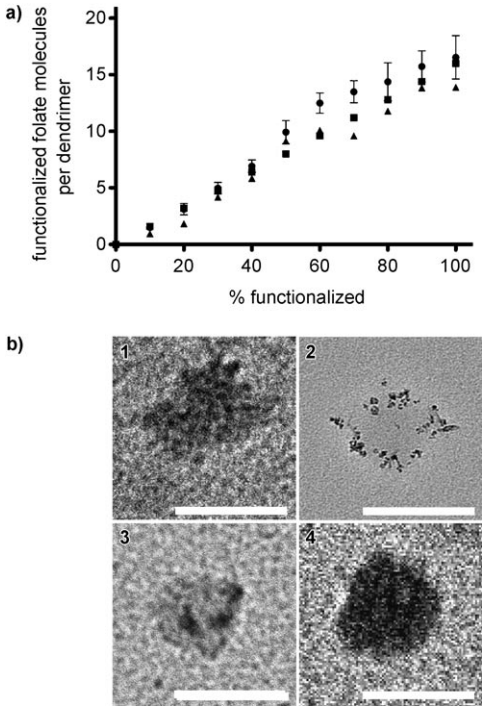

Figure 2. Characterization of LDP mixed micelle system. a) Calculated vs experimental degree of conjugation to dendron. ▲: ^{1}H NMR; ●: UV/Vis; ■: calculated. Experimental values for UV/Vis were calculated using at least three independent sets of measurements (mean ± STD) with free folic acid as the calibration. ^{1}H NMR quantification is described in the Supporting Information. b) TEM images of representative formulations. Clusters of DTPA–Fe^{3+} (DTPA = diethylenetriaminepentaacetic acid dianhydride) on the micelle surface show the formation of mixed micelles. Scale bars = 100 nm. Formulations 10%F–100%mix (1), 20%F–60%mix (2), 30%F–40%mix (3), and 30%F–100%mix (4) are shown.

Supporting Information). The ability of the LDP system to form mixed micelles was confirmed by TEM and FRET (Figure S2d). TEM analysis using Fe^{3+} in the place of folate allow visualization of groupings of "ligands" on the surface of the micelle (Figure 2b).

Using a series of linear dendritic polymers functionalized with 0% to 100% folate groups on the pegylated dendron (0%F to 100%F), we assembled mixed micelles of folate-functionalized polymer with non-functionalized polymer. The resulting micelles present statistically similar amounts of folate but in different cluster arrangements (Figure S2). A series of eight micelle formulations were used: the untargeted control containing unfunctionalized LDP (0%F) used as 100% of the micelle, 0%F–100%mix; and 10%F–100%mix, 20%F–60%mix, 30%F–40%mix, 40%F–30%mix, 60%F–20%, 70%F–20%mix, and 100%F–10%mix are micelle formulations that present stochastic cluster sizes of, on average, 1.5, 3.1, 5.0, 6.9, 12.5, 13.5, and 16.5 folate groups per cluster (Figure S2c). Micelle presenting folates have an average of 2000–2400 groups per micelle and UV/Vis data show statistically similar numbers of folate by one way ANOVA analysis between the different groups at the 95% confidence interval (Table 1). All micelles were 80–90 nm in size. Micelles that present the same amount, but have different spatial arrangements of folate in variable sized clusters, allow meaningful comparisons to be made to determine the effect of folate spatial presentation on cellular internalization.

We used KB[17] cells to evaluate targeting and binding of the micelles to folate receptors that are overexpressed on the cell surface. After a 24 h period of incubation, there was a clear optimum in folate cluster size. The highest cell associated fluorescence was observed for cells incubated with the 20%F–60%mix formulation (Figure 3a). The measured EC50 (concentration producing 50% binding) was observed to be the lowest for the 20%F–60%mix micelle (Figure 3c). We approximated the apparent dissociation

Table 1: Summary of the eight micelle formulations used in this study.[a]

Micelle	Effective diameter [nm]	PDI	Zeta potential [mv]	Folate molecules per micelle
0%F–100%mix	74 ± 1	1.16	−24 ± 3.4	0
10%F–100%mix				1900 ± 250
20%F–60%mix				2200 ± 260
30%F–40%mix				2400 ± 520
40%F–30%mix	90 ± 4	1.2 ± 0.1	−20 ± 0.8	2260 ± 390
60%F–20%mix				2400 ± 400
70%F–20%mix				3100 ± 700
100%F–10%mix				1900 ± 450

[a] 0%F–100%mix is the untargeted control, all other formulations present similar amounts (not statistically different by one-way ANOVA analysis at the 95% CI) of folate but in different cluster sizes and arrangements. Total number of folate presented per micelle (mean ± STD) is calculated based on at least three sets of data (UV/Vis) using an approximate micelle aggregation number of 1000 (based on measured diameters and estimates of LDP unimer dimensions from Materials Studio). Average micelle diameters and zeta potentials are given in mean ± STD of the averages of at least ten individual measurements per micelle. Additional information on diameter, zeta potential information, and folate presentation are shown in Figures S3 and S2b.

Table 2: Apparent K_D, k_{on}, and k_{off} values for the targeted formulations.[a]

Micelle	K_D [M]	K_{off} [s^{-1}]	K_{on} [$M^{-1} s^{-1}$]
10%F–100%mix	$(3.1\pm0.5)\times10^{-9}$	$(1.2\pm0.3)\times10^{-3}$	3.8×10^{5}
20%F–60%mix	$(1.7\pm0.3)\times10^{-11}$	$(1.6\pm0.4)\times10^{-5}$	9.6×10^{5}
30%F–40%mix	$(4.0\pm1.2)\times10^{-11}$	$(3.0\pm1.8)\times10^{-5}$	7.4×10^{5}
40%F–30%mix	$(9.2\pm1.8)\times10^{-11}$	$(8.3\pm0.3)\times10^{-5}$	9.0×10^{5}
60%F–20%mix	$(2.3\pm0.8)\times10^{-10}$	$(4.0\pm1.2)\times10^{-4}$	1.8×10^{6}
70%F–20%mix	$(1.5\pm0.8)\times10^{-10}$	$(1.2\pm0.7)\times10^{-3}$	7.4×10^{5}
100%F–10%mix	$(3.3\pm0.6)\times10^{-9}$	$(9.3\pm1.9)\times10^{-4}$	2.8×10^{5}

[a] K_D and k_{off} were determined experimentally (at least three sets of independent data each), K_{on} was calculated as $k_{on} = k_{off}/K_D$ using mean k_{off} and K_D values.

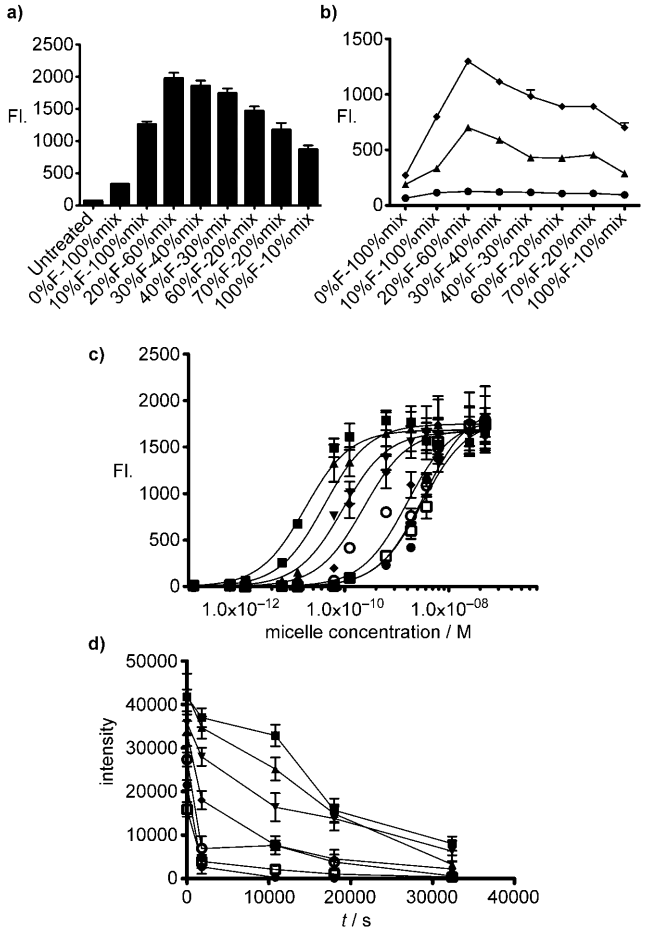

Figure 3. In vitro evaluation of patchy micelles on KB (folate receptor, FR+) and A375 (FR−) cells. a) KB cell-associated fluorescence (Fl.) after 24 h of incubation with micelle formulations. Highest fluorescence was measured from KB cells incubated with 20%F–60%mix formulation (Figure S4a). b) Measured cell-associated fluorescence (Fl.) of KB cells at 5 min (●), 1 h (▲), and 6 h (◆) post incubation. Increase in cell-associated fluorescence between 1 h and 6 h are similar for all targeted formulations, indicating that rate of endocytosis is unaffected by folate presentation. c) The binding avidity (K_D) measured for targeted formulations (●: 10%F–100%mix; ■: 20%F–60%mix; ▲: 30%F–40%mix; ▼: 40%F–30%mix; ◆: 60%F–20%mix; ○: 70%F–20%mix; □: 100%F–10%mix) shows highest avidity with 20%F–60%mix. d) The measured rate of decrease in micelle fluorescence after fixed KB cells pre-incubated to equilibrium with micelles was re-suspended in PBS (phosphate buffered saline). Nonlinear regression analysis using a one-phase exponential decay model gives the apparent dissociation rate constant of micelles from membrane receptors (k_{off}). Calculated values for targeted formulations show the longest dissociation rate with 20%F–60%mix. K_D, k_{off}, and k_{on} values are shown in Table 2. All graphs shown are made with measurements on $n > 3$ independent experiments and are given in mean ± SEM values. Individual flow cytometry measurements were averaged out of 10000 events.

constants of the tested micelles (K_D) by fitting a binding model for site-specific binding to the experimental data. The apparent micelle K_D are given in Table 2. The measured dissociation rate constant (k_{off}) of the different micelles also show that the optimal 20%F–60%mix formulation had the longest dissociation time ($2 \times 10^{-5}\ s^{-1}$; Figure 3d, Table 2). The rate of micelle association was calculated as $k_{on} = k_{off}/K_D$ and was found to be less than 1 order of magnitude apart (Table 2). Confocal analysis and competitive binding experiments confirmed that binding and targeting are folate receptor (FR) mediated and that the mechanism for internalization of targeted LDP is dependent on both energy driven endocytosis and the presence of folate receptors (Figure S5).

To further account for the observed differences in cell targeting, we examined the cell uptake post incubation with micelles as a measure of the kinetics of internalization through the folate receptor (Figure 3b). After a 1 h binding time for internalization, the rate of change in cell-associated fluorescence is not significantly different for all formulations between 1 h and 6 h, indicating that the actual mechanisms of folate internalization are not dependent on ligand presentation; however, the relative levels of cell fluorescence show a strong relationship with their respective binding avidities. All micelle formulations exhibited saturation uptake kinetics at longer time points, suggesting that equilibrium between uptake and secretion was reached by 20 h (Figure S5c). These observations indicate that the enhanced cell targeting of micelles with optimal folate cluster presentation is attributed to having more micelles bind for longer times on the cell surface, which increases the chance for endocytosis.

We estimate that the dendritic element of the LDP has a head group area of 50 to 80 nm^2 and the FR is a protein of ca. 30 kDa that projects a binding area of ca. 13 nm^2 into extracellular space.[18] Examinations of cell membranes that overexpress FR indicate that the FR molecules exist in nanoscale clusters on lipid rafts, with a majority of those clusters consisting of three or more FR molecules.[19–23] Given the available binding space afforded by each dendron, the range of folate–FR interactions that can occur is between 0 and 6, corresponding to LDP conjugated with up to 40% folate. If we were to treat each dendron as a binding entity, LDP–10%F (1.5 ± 0.4 folates/dendron) would bind most weakly to FR clusters and the binding energies of LDP–20%F (3.1 ± 0.9), LDP–30% (5.0 ± 0.9), and LDP–40%F (6.9 ± 0.9) would be greater. Once past the allowable number of ligand–receptor binding events (>LDP–50%F, 9.9 ± 1.8 folates/dendron) within the binding space, the presence of excess ligands clustered in a small binding area would result in steric binding interference, lowering the binding energy.[24]

The cooperativity of this multivalent system can also be helpful in understanding binding effects. This is a negatively cooperative system, as $K_{multivalent} < (K_{monovalent})^{\alpha N}$, where K is the dissociation constant, N is the total number of ligands, and α is the degree of cooperativity (Table 2).[8] In negatively cooperative systems, each successive ligand interaction with a receptor is less favorable than the previous interaction. The calculated degree of cooperativity shows that all formulations were negatively cooperative ($\alpha < 1$ for all formulations), but among the tested micelles, 20%F–60%mix had the highest α, indicating that it is possible to achieve a particular ligand configuration that optimizes the use of each ligand, making the system less negatively cooperative (α closer to 1).

To investigate the significance of cluster presentation in vivo, we delivered formulations 0%F–100%mix, 20%F–60%mix, 60%F–20%mix, and 70%F–20%mix (blood circu-

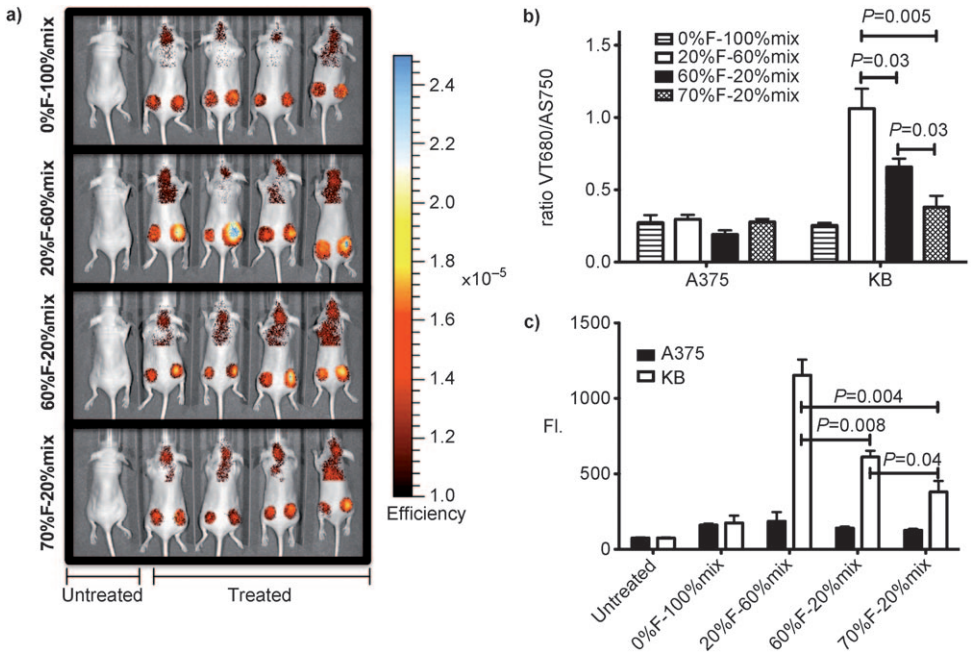

Figure 4. In vivo evaluation of patchy micelles on nude mice bearing two different tumors (right flank: KB, left flank: A375). a) Fluorescence 3D optical imaging of tumored nude mice 48 h after injection with different formulation micelles. Only fluorescence from tumors and a nontumored region of the mice (upper torso) is shown. A side-by-side comparison of VT680 and AngioSence750 fluorescence on the same scale is also shown in Figure S7 to allow identification of the tumors. b) Normalized tumor fluorescence (VivoTag680(VT680)/AngioSense750(AS750)) of tumors ($n=4$) showing the highest in vivo targeting with 20%F–60%mix micelles. Raw fluorescence data is an average of the fluorescence in the region of interest, given in units of efficiency. Ratios are 0.27 ± 0.11, 0.30 ± 0.06, 0.19 ± 0.06, and 0.28 ± 0.04 for A375 tumors and 0.25 ± 0.04, 1.06 ± 0.27, 0.66 ± 0.11, and 0.38 ± 0.16 for KB tumors (0%F–100%mix, 20%F–60%mix, 60%F–20%mix, and 70%F–20%mix, respectively). c) Mean cell-associated micelle fluorescence (Fl.) for cells gated in Q1 + Q3 (see Figure S7) are 160 ± 16, 185 ± 104, 140 ± 17, and 126 ± 15 for A375 tumors and 175 ± 84, 1153 ± 104, 611 ± 71, and 380 ± 126 for KB tumors (0%F–100%mix, 20%F–60%mix, 60%F–20%mix, and 70%F–20%mix, respectively). All data is given in mean ± SEM.

lation half lives 15–20 h; Figure S6) to nude mice bearing KB (FR +) and A375 (FR−) tumors. Figure 4 and Figure S7 show the results from imaging 48 h after injection of micelles. The highest normalized micelle fluorescence was observed for KB tumors in mice injected with 20%F–60%mix. Ratios for the untargeted formulations and all targeted formulations against A375 tumors were found to be within error. To further localize the micelles within the tumor tissue, flow cytometry analysis was performed on tumor cells isolated from whole tumors. We note that the similar trend in data for flow cytometry analysis and 3-D optical imaging show that at the 48 h time point, the majority of the fluorescence accounted for with tumor imaging were from micelles that have been internalized into tumor cells through specific (substantial) or non-specific mechanisms (minimal). The intravenously delivered targeted formulations were able to substantially internalize in live tumor cells in vivo, resulting in a higher population of cells with a higher fluorescence. Optimal clustering of folate also played an important role in enhancing multivalent folate–FR cluster interactions, with the 20%F–60%mix formulation showing the highest level of fluorescence amongst targeted formulations ($P<0.05$ for all analyses comparing 20%F–60%mix, 60%F–20%mix and 70%F–20%mix).

We have shown that ligand presentation in cluster arrangements is a viable design parameter for increasing the efficacy of targeted nanoparticles. In our experiments, cluster arrangement of folate in an optimal size of ca. 3 enhanced uptake of nanoparticles owing to the resultant higher avidity and longer residence times on the cell membrane. This plays a critical role for in vivo targeting where the percentage of intravenously delivered nanoparticles that reach tumor sites by EPR (enhanced permeation and retention) is often less than 10%ID g^{-1},[25] resulting in a low concentration of nanoparticles in the tumor interstitial made available for uptake by tumor cells. To achieve substantial levels of therapy, the avidity of the delivered nanoparticle must be high enough to be able to bind to receptors under such conditions. The results presented here suggest that a shift in focus in molecularly targeted nanocarriers from ligand density to the specific manipulation of ligand cluster presentation may have important implications on cell targeting and can guide the development of more effective targeted delivery systems. It has also been demonstrated that the modular and tunable nature of the linear–dendritic platform can provide a useful probe to examine the importance of ligand–cluster arrangements for cellular interactions.

Received: June 7, 2010
Published online: August 25, 2010

Keywords: micelles · multivalency · nanoparticles · self-assembly · tumor targeting

[1] P. I. Kitov, J. M. Sadowska, G. Mulvey, G. D. Armstrong, H. Ling, N. S. Pannu, R. J. Read, D. R. Bundle, *Nature* **2000**, *403*, 669.
[2] M. Mourez, R. S. Kane, J. Mogridge, S. Metallo, P. Deschatelets, B. R. Sellman, G. M. Whitesides, R. J. Collier, *Nat. Biotechnol.* **2001**, *19*, 958.
[3] X. Montet, M. Funovics, K. Montet-Abou, R. Weissleder, L. Josephson, *J. Med. Chem.* **2006**, *49*, 6087.
[4] C. W. Cairo, J. E. Gestwicki, M. Kanai, L. L. Kiessling, *J. Am. Chem. Soc.* **2002**, *124*, 1615.

[5] S. André, H. Kaltner, T. Furuike, S. I. Nishimura, H. J. Gabius, *Bioconjugate Chem.* **2004**, *15*, 87.
[6] E. A. L. Biessen, F. Noorman, M. E. van Teijlingen, J. Kuiper, M. Barrett-Bergshoeff, M. K. Bijsterbosch, D. C. Rijken, T. J. van Berkel, *J. Biol. Chem.* **1996**, *271*, 28024.
[7] A. David, P. Kopeckova, T. Minko, A. Rubinstein, J. Kopecek, *Eur. J. Cancer* **2004**, *40*, 148.
[8] M. Mammen, S.-K. Chio, G. M. Whitesides, *Angew. Chem.* **1998**, *110*, 2908; *Angew. Chem. Int. Ed.* **1998**, *37*, 2754.
[9] J. Schlessinger, *Cell* **2000**, *103*, 211.
[10] G. Maheshwari, G. Brown, D. A. Lauffenburger, A. Wells, L. G. Griffith, *J. Cell Sci.* **2000**, *113*, 1677.
[11] L. Y. Koo, D. J. Irvine, A. M. Mayes, D. A. Lauffenburger, L. G. Griffith, *J. Cell Sci.* **2002**, *115*, 1423.
[12] S. Azarmi, W. H. Roa, R. Lobenberg, *Adv. Drug Delivery Rev.* **2008**, *60*, 863.
[13] R. Duncan, *Nat. Rev. Cancer* **2006**, *6*, 688.
[14] R. Duncan, *Nat. Rev. Drug Discovery* **2003**, *2*, 347.
[15] L. Tian, P. T. Hammond, *Chem. Mater.* **2006**, *18*, 3976.
[16] M. D. A. Salazar, M. Ratnam, *Cancer Metastasis Rev.* **2007**, *26*, 141.
[17] Y. Lu, E. Sega, C. P. Leamon, P. S. Low, *Adv. Drug Delivery Rev.* **2004**, *56*, 1161.
[18] J. Holm, S. I. Hansen, M. Hoier-Madsen, H. Birn, P.-E. Helkjaer, *Arch. Biochem. Biophys.* **1999**, *366*, 183.
[19] S. D. Weitman, R. H. Lark, L. R. Coney, D. W. Fort, V. Frasca, V. R. Zurawski, Jr., B. A. Kamen, *Cancer Res.* **1992**, *52*, 3396.
[20] J. J. Turek, C. P. Leamon, P. S. Low, *J. Cell Sci.* **1993**, *106*, 423.
[21] B. A. Kamen, M. T. Wang, A. J. Streckfuss, X. Peryea, R. G. W. Anderson, *J. Biol. Chem.* **1988**, *263*, 13602.
[22] R. J. Lee, P. S. Low, *J. Biol. Chem.* **1994**, *269*, 3198.
[23] S. Hong, P. R. Leroueil, I. J. Majoros, B. G. Orr, J. R. Baker, M. M. Banaszak Holl, *Chem. Biol.* **2007**, *14*, 107.
[24] W. S. Hlavacek, R. G. Posner, A. S. Perelson, *Biophys. J.* **1999**, *76*, 3031.
[25] H. Maeda, J. Wu, T. Sawa, Y. Matsumura, K. Hori, *J. Controlled Release* **2000**, *65*, 271.
[26] M. Pittelkow, R. Lewinsky, J. B. Christensen, *Org. Synth.* **2007**, *84*, 209.
[27] N. Parker, M. J. Turk, E. Westrick, J. D. Lewis, P. S. Low, C. P. Leamon, *Anal. Biochem.* **2005**, *338*, 284.
[28] C. A. Ladino, R. V. J. Chari, L. A. Bourret, N. L. Kedersha, V. S. Goldmacher, *Int. J. Cancer* **1997**, *73*, 859.

